Title
HIGH EFFICIENCY GAMMA CONVERTERS AND THEIR APPLICATION IN A MWPC POSITRON CAMERA

Author
Chu, D.

Publication Date
1976-10-01

To be presented at the Symposium on
Medical Radionuclide Imaging,
Los Angeles, CA, October 25 - 29, 1976

LBL-5516 c.1
IAEA-SM-210/63

HIGH EFFICIENCY GAMMA CONVERTERS AND THEIR APPLICATION IN A MWPC POSITRON CAMERA

D. Chu, K. C. Tam, V. Perez-Mendez, S. N. Kaplan,
C. B. Lim, R. Hattner, L. Kaufman, D. Price, and Sybil Swann

October 1976

Prepared for the U. S. Energy Research and
Development Administration under Contract W-7405-ENG-48

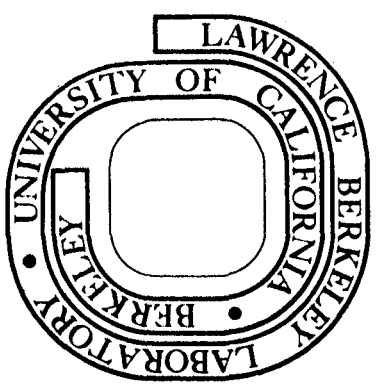

LBL-5516 c.1

DISCLAIMER

LBL-5516
IAEA-SM-210/63

Symposium on Medical Radionuclide Imaging
October 25-29, 1976
Los Angeles, California

High Efficiency Gamma Converters and Their Application in a MWPC Positron Camera*

D. Chu, K.C. Tam, V. Perez-Mendez† and S.N. Kaplan

Lawrence Berkeley Laboratory

and

C.B. Lim, R. Hattner, L. Kaufman,
D. Price and Sybil Swann

University of California, San Francisco

Abstract

Honeycomb structured lead γ-ray converters have been developed and coupled with Multiwire Proportional Chambers to produce a position-sensitive hybrid detector for spatial localization of MeV range γ rays. Two such detectors operated in time coincidence mode function as a large-area large-solid-angle positron camera. The sensitivity of the camera system is measured to be 1 600 counts/min-μCi, corresponding to a detection efficiency of 5.5% per detector. Images of phantoms and clinical objects are obtained by using the back-projection reconstruction method, and the results demonstrate the tomographic capability of such a positron camera system.

A design analysis of the γ converter is presented, the detection efficiencies of converters of various dimensions are measured, and the results agree quite well with calculation. Further improvements in converter efficiency can be expected with modifications in the converter designs based on the concepts of enhanced surface area and uniformity of electron extraction field. The new converters under consideration are made of small-diameter high-lead-content lead glass tubing made conductive by hydrogen reduction treatment.

---

* This work was done with support from the U. S. Energy Research and Development Administration.

† Also at University of California, San Francisco.

Introduction

The use of multiwire proportional chambers (MWPC) for detection and spatial localization of gamma radiation is limited by the low conversion efficiency of the chamber gas. Only for low-energy gamma radiation does the combination of a noble gas of high atomic number with pressurization produce a satisfactory detection efficiency. Xenon at 4 atmospheres has been used for 60 keV gammas to obtain a detection efficiency of 50%. But as the energy of the gamma radiation increases, the detection efficiency decreases rapidly, and the spatial resolution degrades because the energetic conversion electrons travel farther in the gas. If a solid plane converter is coupled to the active region of a MWPC, gamma rays interact with the solid converter, yielding conversion electrons. Some of the conversion electrons escape the solid medium and enter into the gas regions, producing ionization electrons which are detected, as in the case of a conventional MWPC. The useful thickness of such a plane converter is limited by the maximum range of the conversion electrons. This thickness is usually very small, and the problem can be visualized as a surface phenomena. A structured gamma converter such as a honeycomb, can provide an enhanced surface area as well as restricting the range of conversion electrons. In part (I), the gamma detection efficiency of a honeycomb converter is described, and detailed construction of such converters is presented. The detection efficiencies for various converter configuration are measured and compared with the calculated results. In part (II), a positron camera using MWPC-gamma converters as detectors is described. The characteristics and the performance of the positron camera are evaluated.

Part I. Gamma Converter

I.1. Gamma Converter Efficiency

The efficiency of a structured gamma converter depends on the following:

(a) The probability of electron-producing gamma interactions in the converter material. This is a function of the total g/cm^2 of the converter.

(b) The escape probability of these conversion electrons* into the detector gas. This is a function of the mean distance to an escape surface and the range of the conversion electrons.

I.1.1. Conversion yield

Consider an array of square-cross-section cells with dimensions as shown in Fig. 1. Conversion electrons, resulting from either photoelectric or Compton interactions of incident gammas with the material, have to traverse the solid and escape into the gas region where ionization can occur. In general, a photon will traverse several cells, depending on the orientation of the converter with respect to source position (Fig. 2). A simple model is first described to specify the important

*For convenience these electrons will be referred to as "conversion electrons"--although this is not the conventional meaning of the expression.

parameters in the consideration of high conversion yields for gamma converter designs. This will be followed by a more precise analysis and expressions for calculating the conversion yield.

For a cell, Fig. 1, with total surface area A_s and cross section A_c, the probability of producing secondary ionization electrons per gamma is

ε = interaction probability per unit cross section × probability of escape of conversion electrons.

$$= V_{eff}\ (N\sigma)\ \bar{P}_{esc} / A_c = (A_s T)\ (N\sigma)\ \bar{P}_{esc} / A_c$$

$$= 4Ht\ (L - T)\ (N\sigma)\ (\bar{P}_{esc}) / (L + 2T)^2, \qquad (1)$$

where V_{eff} is the effective conversion volume, N is the number of atoms per unit volume, σ is the conversion cross section per atom, and $\bar{P}_{esc}$ is average escape probability for conversion electrons produced within the wall thickness, T. H is the height of the converter and L is the width of a side of a square cell. For a cell of width L >> T, Eq. (1) simplifies to

$$\varepsilon = \frac{4\ HLT}{L^2}\ (N\sigma)\ (\bar{P}_{esc})$$

$$= \frac{4H}{L}\ T(N\sigma)\ (\bar{P}_{esc}). \qquad (2)$$

The most direct way to increase the conversion yield is to increase the ratio of H/L, the height of the converter versus the cell width. As we shall see in the next sections, the width L is limited by the collection efficiency of the ionization electrons and the minimum threshold for detection. This simple model does not include the effects of angular dependence nor the detailed profile of conversion electron escape. The following more precise expression was used in the actual calculation of gamma converter efficiency:

$$\varepsilon = \Sigma n_j = \sum_{j=1}^{N} \sum_{i=1}^{2} \int_0^T Q_{ij}\ \frac{(L + 2x)}{(L + T)T}\ dx\ P_{esc}\ (x, E_i), \qquad (3)$$

where i indicates the type of interaction (photoelectric and Compton), n_j is the probability of emitting an electron into the j-th cell space, P_{esc} is the escape probability of electron with energy E_i at x, Q_{ij} is the probability that an i-th type electron is produced in cell j, and N is the total number of cells.

In the case of a point source with a wide angular spread, Fig. 2, the average number of electrons produced per gamma over the solid angle subtended by the source and converter is calculated. For a given geometry, the summation over j reduces to a geometric factor, G (Ref. 2). The simplified expression for the conversion yield, ε, for a point source is,

for example,

$$\varepsilon = 2G \left[\sum_{i=1}^{2} \sigma_i \rho T \int_0^T \frac{(L + 2x)}{(L + T)T} \, dx \, P_{esc} \, (x, E_i) \right] . \qquad (4)$$

In order to calculate the conversion yield, an analytic form for the escape probability is required.

Spencer [3] used a numerical method of spatial moments to evaluate P_{esc}:

$$P_{esc} \, (x, E_i) = \exp A \left[1 - \frac{x}{R(E_i)} \right]^p \exp \left[- \frac{A}{1 - \frac{x}{R(E_i)}} \right] , \qquad (5)$$

where A is a function of source energy and scattering material, P is a constant, and $R(E_i)$ is the residual range defined and tabulated by Nelms [4]. The value of the coefficients A and p can be obtained from experimental data. The electron escape probability $P_{esc}(x, E_i)$ for a number of materials has been measured by Seliger [5], with a 2π β counter with high detection efficiency, down to electron energies of a few hundred electron volts. Equation (5) is relatively insensitive to the value of P.

The residual range $R(E_i)$ is determined from the kinetic energy of the two types of conversion electrons, photoelectric and Compton. In photoelectric interactions, the energy of conversion electrons is given by the difference between the incident gamma energy and the binding energies of the electrons, $E_p = E_\gamma - E_k$. Contribution from L and M shells should also be included for high-Z materials. Since the Compton interaction yields a continuous spectrum, an average Compton electron energy, $\bar{E}_i$, is used to calculate the escape probability.

I.1.2. Intrinsic conversion yield

In the simple case where the converter is a plane surface of thickness greater than the optimum thickness and the detection of conversion electrons is restricted to one side of the converter, as in the case of Geiger counters, the conversion yield, ε, is given by

$$\varepsilon = \frac{\sum_{i=1}^{2} \iint \sigma_i \rho \exp \, (-\sigma_T \rho x \sec\theta) \, \sec\theta \, P_{esc} \, (x, E_i) \, dx d\Omega}{\int d\Omega} . \qquad (6)$$

The intrinsic conversion yield of various materials for different energies can now be calculated with the analytical form for the electron escape probability. The intrinsic conversion yield of various types of cathode materials have also been measured [6]. Both measured and calculated results of ε as functions of gamma energy are compared in Fig. 3.

I.1.3. Extraction efficiency

In the previous sections we have considered the probability of conversion electron emission into the gas region within the cells. The number of ionization electrons collected is dependent on the profile of the extraction electric field. For a given chamber the number of ionization electrons collected multiplied by the gain of the chamber (typically 10^4 - 10^6) must exceed the input noise level of the readout amplifier in order for an event to be detected.

In order to extract ionization electrons from the gas regions within the cells, an electric field has to be applied across the converter. To estimate the average number of ionization electrons produced within a cell and the influence of electric field profiles on the extraction efficiency, we assume a cylindrical cell geometry. Conversion electrons emitted from the wall produce ionization tracks of various lengths, depending on the orientation of these tracks. This track-length distribution, f(r), has been calculated for a cylinder [7] and the result is shown in Fig. 4. The conversion electron range is assumed to be long compared to the cylinder diameter (this is the case for a cylinder radius on the order of 1-2 mm and electron energy greater than 10 keV). If we define a detection probability, $D(r_t)$, as the probability of detecting an escaped conversion electron from a gamma interaction, then

$$D(r_t) = \int_{r_t}^{r_{max}} T(r)\, dr,$$

where T(r) is the track length distribution function and r_t is the threshold track length. In the case mentioned above, the extraction field is assumed to be uniform and there is no loss of ionization electrons in the drifting process.

In a gamma converter where the conversion material is a metal, a drift field is produced by electrically biasing a series of strips with insulating materials between them. Such an extraction field is non-uniform, and a typical electric field profile is shown in Fig. 5. From the electric field profile, it can be seen that some ionization electrons are lost in the drifting process due to the termination of the field lines on the walls. The space within a cell can then be approximated by two concentric cylindrical regions, an inner cylinder (of radius $\bar{r}$) where electric field lines are continuous along the length of the cell and an outside cylindrical shell (of outer radius R) where field lines terminate on the wall (Fig. 6). In this model the probability of detecting a gamma ray which has produced a conversion electron is equal to the probability that the ionization track intersects the inner cylinder (intersection probability), and produces within it a sufficient number of secondary electrons (detection probability). The ionization electrons released as a result of the interaction of the conversion electrons with the gas in the chamber will tend to spread out by diffusion in the course of their motion towards the anode wires. However, in our case, the rate of diffusion is assumed to be small and ionization electrons are considered to drift along the field lines. The electrons in the central region are extracted, while electrons in the outer cylindrical volume are lost. For a cosine emission distribution from the wall, the

probability that an ionization track will intersect the inner cylinder is:

$$P(\bar{r}/R) = 1 - \frac{4}{\pi} \int_0^{\mu_0} \mu \cos^{-1}\left[\mu\bar{r}/R\ (1-\mu^2)^{1/2}\right] d\mu \ , \qquad (7)$$

where

$$\mu_0 = \left[1 + (\bar{r}/R)^2\right]^{-1/2} .$$

The track-length distribution in the inner cylinder is assumed to be that shown in Fig. 4. In this case the detection is:

$$D(r_t) = \int_{r_t}^{\infty} T(r)dr \ .$$

Total converter efficiency is then expressed as a product of conversion yield, intersection probability, and detection probability:

$$\varepsilon_t = \varepsilon \times P(\bar{r}/R) \times D(r_t) \ .$$

Results of the calculated and measured converter efficiencies will be presented in the following sections.

I.2. Converter Design and Construction

I.2.1. Converter design

The conversion yield, ε, is shown to be proportional to the ratio of cell height (H) to width (L), Eq. (2). The cell width is limited by the extraction efficiency, which has already been discussed. The limitation on the height of a converter is more specifically related to the particular application. For example, the time required for ionization electrons to drift from inside the cells into the multiplication region of the chamber is dependent on the converter height. This puts a practical limit to the converter height if a fast electron drift time should be needed. Another factor that has to be considered in an efficient converter design is the self-attenuation of the cell walls. For low-energy gammas (<100 keV), and for a converter made from high-Z material, gamma attenuation by the walls is considerable and the converter efficiency can deviate from the simplified expression given in Eq. (2). The more precise expression, Eq. (4), should be used to calculate the optimum thickness of the converter wall.

Lead, being the least expensive and most readily available high-Z material, was the basis for two converters considered here, one made from lead strips on a plastic backing and the other from lead glass.

(a) Lead honeycomb converter

One approach to making a structured converter with thin walls is to assemble corrugated metal-coated plastic strips into a honeycomb structure. These strips were made by plating lead onto copper which is bonded to Mylar. Because an extraction field is required for electron drifting, each strip of lead is divided into several layers with insulating material between layers, and a graded voltage is applied across the converter through a resistor chain. The detailed construction method is presented in the next section. Using this method, a converter of large dimensions can be made quite easily, and this is the main advantage of such a construction. There are two disadvantages, however, to this design. First, it is technically difficult to construct a small cell-size honeycomb. Second, due to the non-uniformity of the electric drift field, a portion of the ionization electrons is lost in the drifting process.

(b) Lead glass converter

In order to have a uniform drift field, the converter wall material should be resistive, and in order to have high conversion yield, a high-Z material is required. Glass tubing containing PbO satisfies both of these requirements. Though the intrinsic conversion yield of lead glass is lower than that of pure lead, a more uniform drift field and, consequently, better extraction efficiency can be obtained with the lead glass converter. A comparison of conversion yield of lead glass of various compositions with that of lead is shown in Fig. 7. The total detection efficiency of a lead glass converter, however, is comparable to that of the lead honeycomb converter when the extraction efficiency is taken into consideration. The calculation of the lead glass conversion yield as a function of wall thickness for various gamma energies is shown in Fig. 8. As expected, the optimum wall thickness diminishes rapidly with decreasing gamma energy

I.2.2. Converter construction

(a) Lead honeycomb converter

The optimum thickness of cell walls made of lead was calculated to be 75 microns for 511 keV gammas. Photoetching and electroplating methods were employed to construct these thin-walled converters. Bands of copper were photoetched on sheets made of 50 microns of Mylar, clad on both sides with 50 microns of copper. Subsequently, a layer of lead 75 microns thick was electroplated onto the copper. Strips of selected width were cut from these sheets and corrugated with two meshing gears. The strips were then soldered together to form a honeycomb structure. Metal bands at the same height were connected by a common bus wire. A drift field is provided to each cell by applying graded voltages to the bus wires (Fig. 9).

(b) Lead glass converter

Thin-walled lead oxide glass tubes (30% - 80% by weight) were fused together at 600°C, using a carbon mold. The fused assembly was then sliced to the desired height and cleaned. The converter was again heated in hydrogen at 350-420°C for 1-2 hours. The PbO was reduced,

forming a resistive surface layer. Silver conductive paint was then applied to both surfaces of the converter, so that voltage could be applied through a wire epoxied to the surface, Fig. 10.

I.3. Test Chamber and Results

A MWPC test chamber with 25 × 25 cm sensitive area was used to measure the detection efficiency of 511 keV gammas for converters of various cell dimension. Test converters 15 × 15 cm were placed parallel to the cathode plane of the chamber. The detection efficiencies of various converters were measured by using a Na-22 positron source. Corrections were made to the raw counts, since a 1.27 MeV gamma is also emitted with every pair of annihilation gammas. Table I compares the calculated values of ε_t with the measured detection efficiencies for various cell dimensions. As can be seen from the table, the measured extraction efficiencies which vary between 0.73 - 0.83 are in good agreement with the calculated values.

Table I. Converter Efficiency Measurements

Converter cell	Surface area / Cross sect.area	ε_t(cal.) (%)	ε(exp.) (%)	ε(exp.) / plane	Measured Extraction Efficiency
Lead honeycomb					
Pb (511 keV gamma)	$4LH/L^2$				
Plane converter	1	0.26	0.26	1.0	1.00
3mm×3mm×12mm	16	3.12	3.20	12.3	0.76
2.2mm×2.2mm×12mm	22	4.29	4.20	16.2	0.73
2mm×2mm×4mm	8	1.56	1.55	5.4	0.74
Lead glass *	1	0.17	0.17	1.0	1.00
2mm×2mm I.D.×15mm	13	1.98	1.90	11.0	0.90

*This lead glass tubing contained only 30% PbO by weight and its efficiency is included here merely for verifying the accuracy for calculations and measurements. For γ imaging applications we propose to use thin walled (t_{wall} ~ 100 microns) glass with lead concentrations 50-80% by weight.

Part II. A MWPC-Gamma Converter Positron Camera

By using the directional property of the monoenergetic annihilation gammas (511 keV) from a positron emitter, determination of activity distribution is accomplished using two position-sensitive detectors operating in coincidence without the use of collimators. Reconstruction can be done by the back-projection method [8] or by suitable algorithms for three-dimensional reconstruction [9, 10].

A collimatorless positron imaging system has inherently good sensitivity, and further gamma utilization can be achieved if the camera has a large field of view. A large-area detector can be made using MWPC equipped with gamma converters at relatively low cost. Such a hybrid detector offers excellent spatial resolution as well as uniformity of response. The disadvantages are suboptimal detection efficiency and no energy resolution. However, these drawbacks are offset by both the favorable characteristics of the detectors and by the ideal matching of these detectors to the physical processes involved in positron imaging.

II.1. Positron Camera Description

A schematic representation of the positron camera system is shown in Fig. 11. Signals for each coincident event are electronically processed, and the positions of the gamma interaction sites are digitized and transferred via the computer memory to a mass data storage disc unit. The MWPC-gamma converter positron imaging system consists of three major groups of hardware. The first group includes MWPC chambers, gamma converters, and delay lines used for the localization of gamma interaction sites [13]. The second group of hardware includes the electronic components for signal processing. The third group of hardware consists of a PDP 11/20 computer with peripherals. The complete camera system is shown in Fig. 12.

The vital components of this camera system are the detectors. Each detector has two MWPCs with 48 × 48 cm sensitive area coupled to lead honeycomb converters. At present, each detector has three converters. Each lead converter consists of four 3mm-high bands. Figure 13 shows the detector assembly with the window removed.

II.2. Characteristics and Performance of Positron Camera

The camera performance characteristics which would dictate the qualities of the images are as follows:

(a) Sensitivity of the imaging system (counts/min-μCi)

(b) Spatial resolution of the imaging system.

Sensitivity

The sensitivity, S, for coincident detection is defined as counts/min-μCi:

$$S = 2.22 \times 10^6 \, G\varepsilon^2 \, , \tag{8}$$

where G is the geometric acceptance, and ε is the detection efficiency

of each detector. A positron emitter (Cu-64) of known activity is placed at the center of the mid-plane between the detectors. From Eq. (8) and the response data for Cu-64 sources (which include the effects of attenuation by the 2.5 mm aluminum entrance windows on each side), we find S = 1 600 counts/min-μCi, and an effective detection efficiency for each side of ε = 5.5%.

Spatial resolution

Using Cu-64 line sources ($E_{\beta+}$ = 656 keV), spatial resolution of 6 and 7 mm FWHM are found for sources embedded in 1.25 and 10 cm of lucite, respectively, Fig. 14. Thus scattering has relatively small effect on the spatial resolution, and the lack of energy resolution in the MWPCs does not significantly alter the performance of the system.

External Scattering

The effects of scattering material in the path of the annihilation photons have been investigated. As expected, the number of background events is increasing. The energy resolution capability of a scintillation camera would not significantly improve this situation. This can be seen as follows: for 511 keV photons, the major interaction mechanism in tissue is Compton scattering, which at this energy shows a high degree of forward peaking. At 511 keV, a 15% energy loss (which would be accepted by the usual scintillation camera pulse-height window) corresponds to scattering through 35 degrees. Thus, most scattered events are accepted by both the MWPC and scintillation positron cameras.

Imaging Results

The following images obtained with the MWPC positron camera using the back-projection method for display, demonstrate the capabilities of the system (no field uniformity correction or digital processing have been performed on these images). Figure 15 shows the image of a 1.5 cm diameter Cu-64 ring. Figure 16 shows two Cu-64 wire sources separated by 1 cm. Figure 17 shows the tomographic reconstruction of the upper part of a dog labelled with F-18. Figure 18 shows both the tomographic reconstruction images of the brain labelled with Ga-68 DTPA and the images obtained with a conventional gamma camera and with an EMI scan.

Conclusion

The detection efficiency of gamma radiation with MWPC detectors can be improved by using structured solid converters which are particularly effective for gamma energy above 100 keV. Two converter designs, one made of lead and the other of lead glass, were described. With lead glass converters, a more uniform extraction field is obtained and, in addition, small cell size converters can be made easily. The lead glass converter that was used in our preliminary measurement has a wall thickness much greater than the optimum value. The detection efficiency obtained agrees with the calculation. Another approach, which is now under investigation, is the use of microchannel plate converters. These plates, which can be made of lead-bismuth oxide glass, have hole diameters between 20 - 200 microns [12]. If these devices are operated in a vacuum ($<10^{-5}$ Torr), electron multiplication of 10^6 is obtainable. The cascade

electrons, in this case, are collected by a set of cross-grid wires placed over the converter, and the charge from each event is shared by a pair of orthogonal wires. Coordinate readout can be accomplished by the conventional delay line method.

A positron camera using MWPCs coupled to lead honeycomb converters has been developed. The converters used have cell size of approximately 3.5 mm, and the system spatial resolution obtained is 6-7 mm FWHM. The system detection efficiency measured for each detector is 5.5%. Due to the camera's large solid angle coverage, a high sensitivity of 1600 counts/min-μCi is observed. However, due to the accidental and scattering coincidence, the present maximum data rate is 34 K cpm. After initial tests with phantoms and animals, the camera has been used in clinical trials with brain imaging. The results demonstrated the tomographic capability of such a MWPC - gamma converter positron camera. The converter was made from lead glass tubing (30% PbO), supplied by Corning Glass Co.

In order to upgrade the camera performance, in terms of increasing the sensitivity, maximum count rate capability, and spatial resolution, the coupling of lead glass and microchannel plate converter to the positron camera will be investigated. A projection in the improvement of the camera sensitivity due to various converter modifications is shown in Table II. Programs are also being developed to remove the blurring effect of the off-focal plane activity on the image by using three-dimensional image reconstruction algorithms.

Table II. Effect of Proposed Modifications on MWPC Positron Camera Performance.

1. Present Camera (2 honeycomb converters each side)

Height of converter	(H = 15 mm)	
Cell size	(L = 3.5 mm)	
Detection efficiency		= 4.5%
Sensitivity		= 900 counts/min-μCi
Count rate with 10% accidentals		= 400 counts /sec

2. Camera with 8 converters (4 honeycomb converters each side)

Height of converter	(H = 12 mm)	
Cell size	(L = 2.5 mm)	
Detection efficiency		= 11%
Sensitivity		= 5.4K counts/min-μCi
Count rate with 10% accidentals		= 2.4K counts/sec

3. Lead-Glass converters*(4 converters each side)

PbO concentration	(50%)	
Height of converter	(H = 15 mm)	
Cell size	(L = 2mm)	
Detection efficiency		= 22%
Sensitivity		= 22K counts/min-μCi
Count rate with 10% accidentals		= 9.6K counts/sec

4. Micro-channel plate converters (2 converters each side)

PbO concentration	(50%)	
Height of converter	(H = 5 mm)	
Cell size	(L = 10 μm)	
Detection efficiency		= 30%
Sensitivity		= 40K counts/min-μCi
Count rate with 10% accidentals (with dead time of 1 μsec, resolving time of 1 nsec)		= 46K counts/sec

*The wall thickness of the glass tubing is 100-150 microns.

REFERENCES

[1] KAPLAN, S.N., KAUFMAN, L., PEREZ-MENDEZ, V., VALENTINE, K., Nucl. Instrum. Methods 106 (1973) 397.

[2] CHU, D., TAM, K.C., PEREZ-MENDEZ, V., LIM, C.B., LAMBERT, D., KAPLAN, S.N., High efficiency collimator converters for neutral particle imaging with MWPC, IEEE Trans. Nucl. Sci. 23 (1976) 634.

[3] SPENCER, L.V., Theory of electron penetration, Phys. Rev. 98 (1955) 1597.

[4] NELMS, A.T., Nat. Bureau of Standards (Washington) Circ. 577 (1956).

[5] SELIGER, H.H., Backscattering of positrons and electrons, Phys. Rev. 88 (1952) 408.

[6] BRADT, H., Helv. Phys. Acta. 19 (1946) 77.

[7] CASE, K.M., DE HOFFMAN, F., PLACZEK, G., "Introduction to the theory of neutron diffusion," U.S. AEC Report, Section 10 (1953) Vol. 1.

[8] ATKINS, F.B., OPPENHEIM, B.E., HARPER, P.V., Image reconstruction using a positron camera, Digest of the Fourth International Conference on Medical Physics, Vol. 32, Sect. 14.2 (1976).

[9] MACDONALD, B., CHANG, L.T., PEREZ-MENDEZ, V., Three dimensional image reconstruction with large area positron cameras, Digest of the Fourth International Conference on Medical Physics, Vol. 32, Sect. 14.5 (1976).

[10] CHU, G., TAM, K.C., Three dimensional imaging in the positron camera using Fourier techniques, Physics in Medicine and Biology, 1976.

[11] GROVE, R., PEREZ-MENDEZ, V., SPERINDE, J., STOKER, G., LBL-1035, UC-37 Instruments, T10-4500 (59th Ed.).

[12] RUGGIERI, D.J., Microchannel plate imaging detectors, IEEE Trans. Nucl. Sci. 19 (1972) 74.

FIGURE CAPTIONS

Fig. 1. Schematic of a square-cross-section cell array with unit cell dimension specified.
Fig. 2. Detector geometry for a point source with wide angular spread.
Fig. 3. Measured (Ref. 6) and calculated results of intrinsic conversion yield in various materials as fractions of gamma energy.
Fig. 4. The track-length distribution in an infinite cylinder of radius R.
Fig. 5. Schematic configuration of lead converters showing the electric drift field lines.
Fig. 6. A concentric cylindrical geometry showing an inner cylinder of radius $\bar{r}$, and outer shell of radius R.
Fig. 7. Comparison of conversion yield of lead glass converter and lead converter.
Fig. 8. Conversion yield of lead glass as a function of wall thickness for various gamma energies.
Fig. 9. A section of the layered honeycomb-shaped gamma converter.
Fig. 10. A section of the fused lead glass converter.
Fig. 11. Schematic configuration of the MWPC positron camera.
Fig. 12. The MWPC positron camera. Left, detection system; center, CAMAC coordinate processing electronics; right, PDP 11/20 computer.
Fig. 13. Detector assembly showing the MWPC chamber and the gamma converter.
Fig. 14. (a) A Cu-64 line source in 1.25 cm of lucite, showing a spatial resolution of 6 mm FWHM.
(b) Same source in 10 cm lucite. The resolution is 7 mm FWHM.
Fig. 15. 1.5 cm diameter Cu-64 ring source.
Fig. 16. Two Cu-64 line sources separated by 1 cm.
Fig. 17. F-18 bone scan of a dog 2 hours after injection of 800 μCi. Images were reconstructed on planes separated by 2 cm.
Fig. 18. Right parietal oligodendroglioma. Note central necrosis evident in the 5.0 cm plane, not apparent in conventional scan, lower left, but confirmed in EMI scan, lower right.

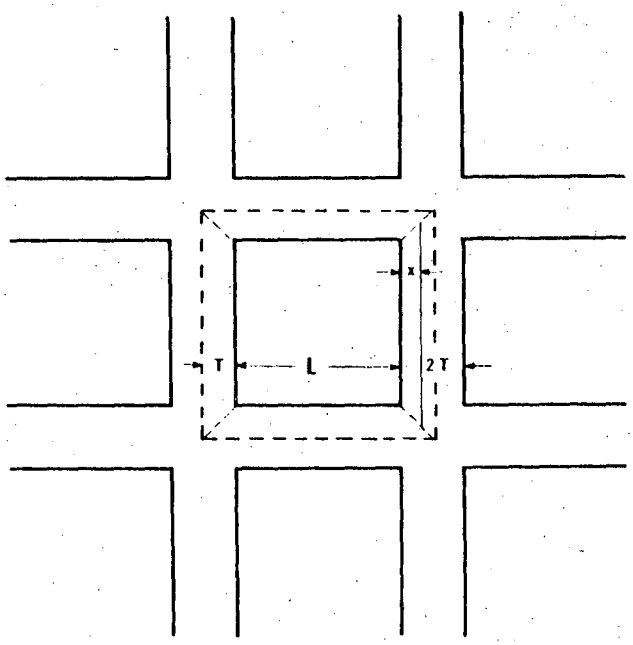

Fig. 1

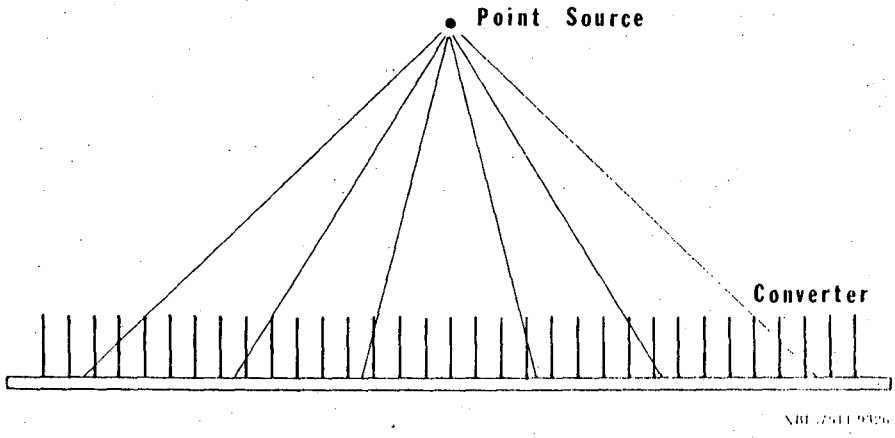

Fig.2

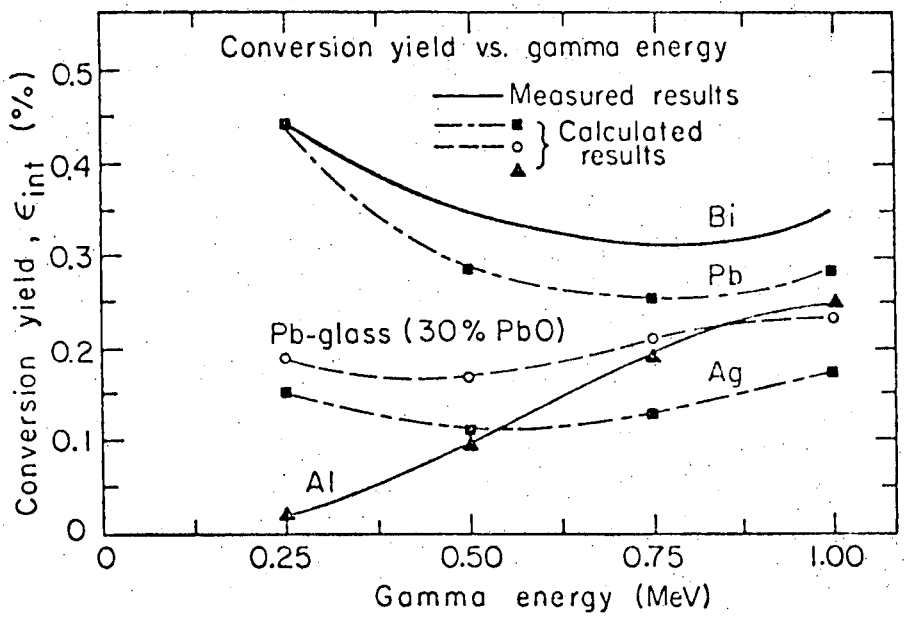
Conversion yield vs. gamma energy
Measured results
Calculated results
Bi
Pb
Pb-glass (30% PbO)
Ag
Al
Conversion yield , ϵ_{int} (%)
0.5
0.4
0.3
0.2
0.1
0
0
0.25
0.50
0.75
1.00
Gamma energy (MeV)

Fig. 3

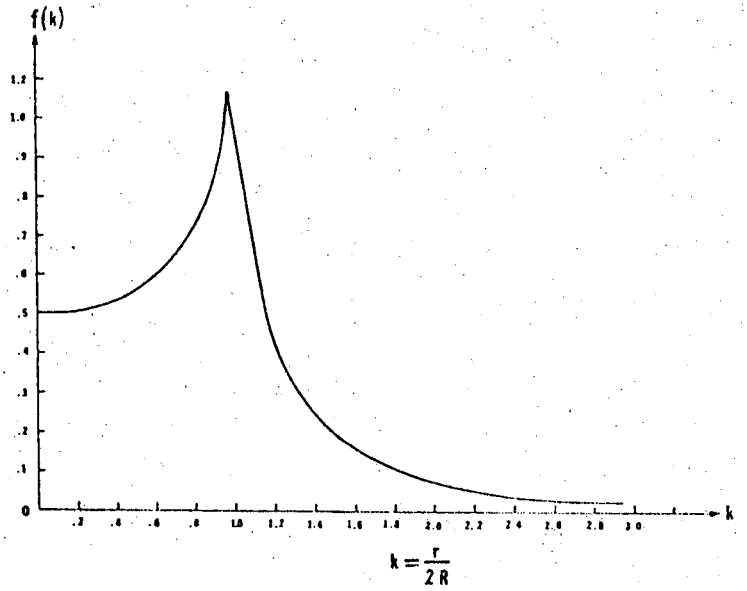
f(k)
k
$k=\frac{r}{2R}$

Fig. 4

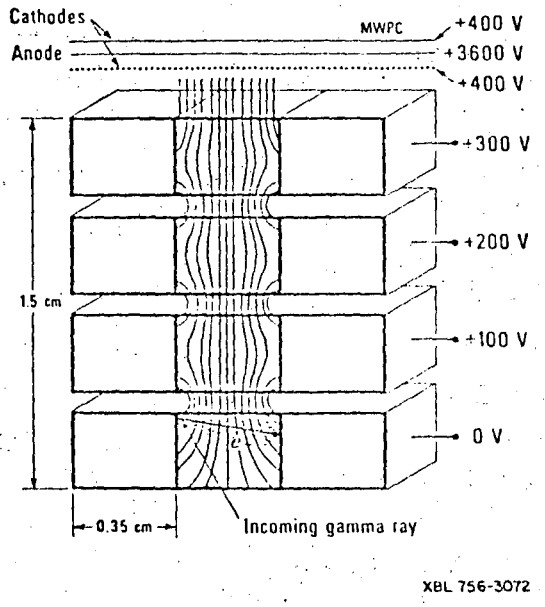
Cathodes
Anode
MWPC
+400 V
+3600 V
+400 V
+300 V
+200 V
+100 V
0 V
1.5 cm
0.35 cm
Incoming gamma ray
XBL 756-3072

Fig. 5

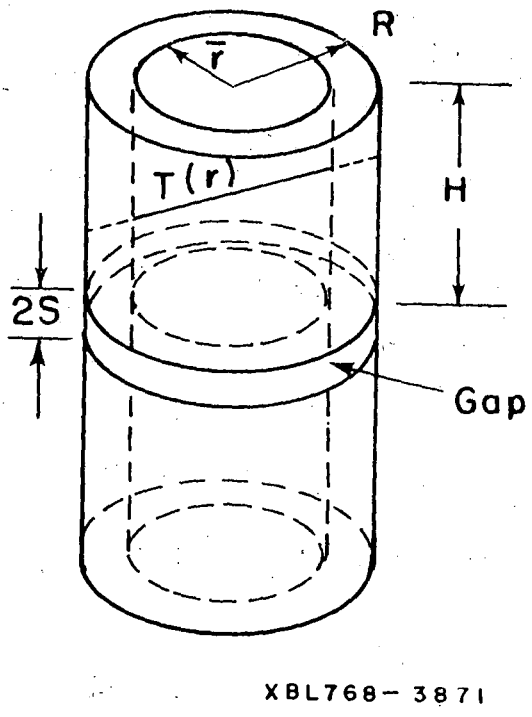
R
r̄
T(r)
H
2S
Gap
XBL768-3871

Fig. 6

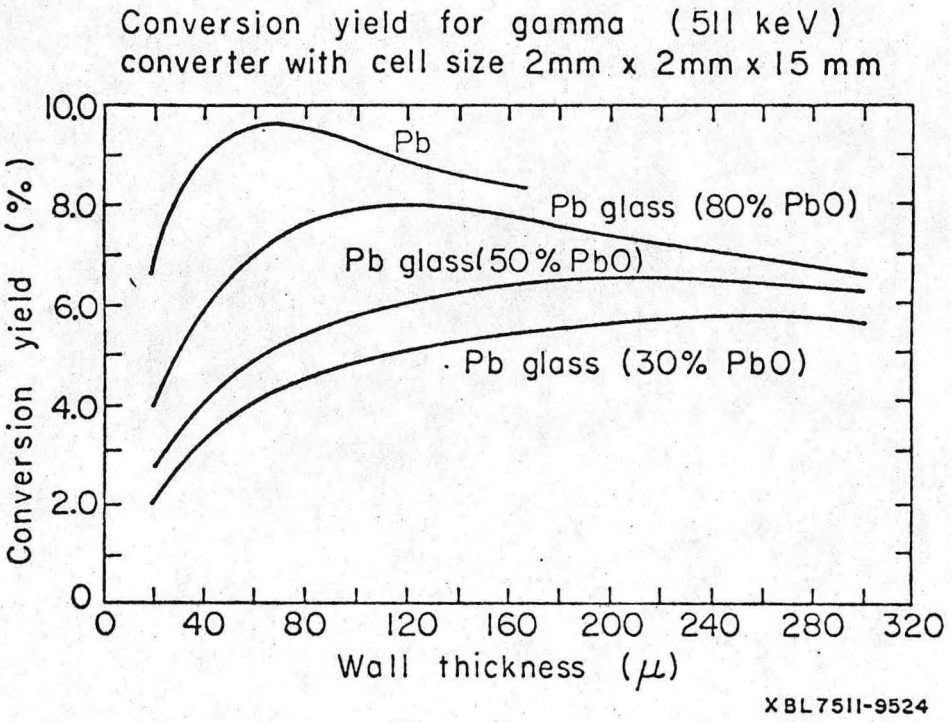

Fig. 7

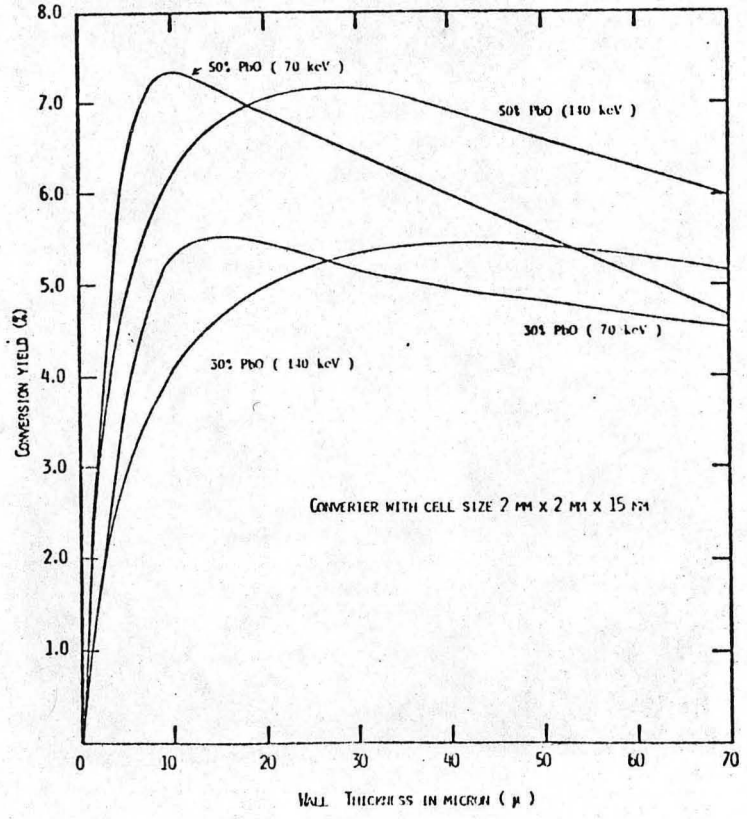

Fig. 8

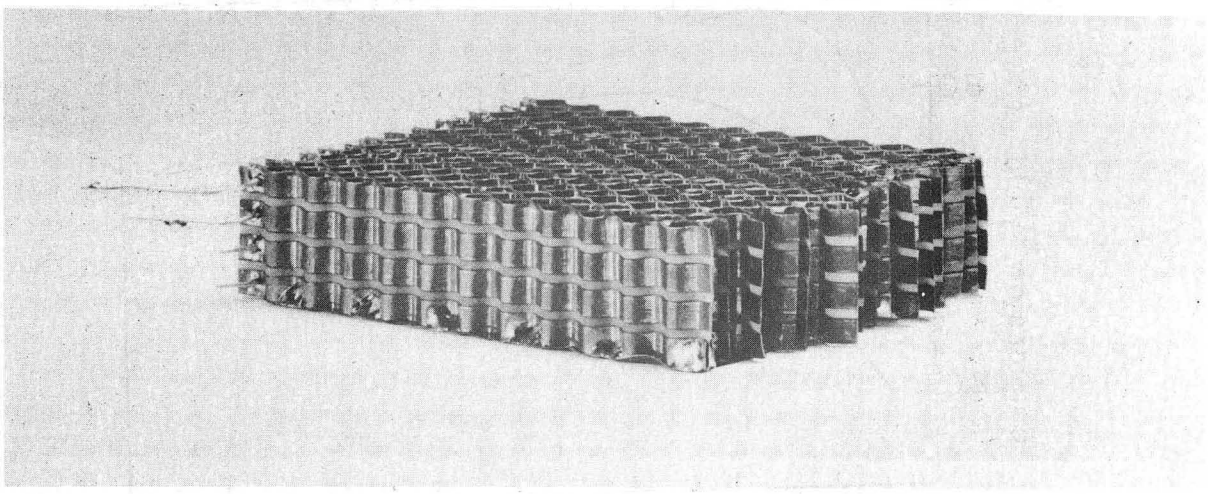

Fig. 9

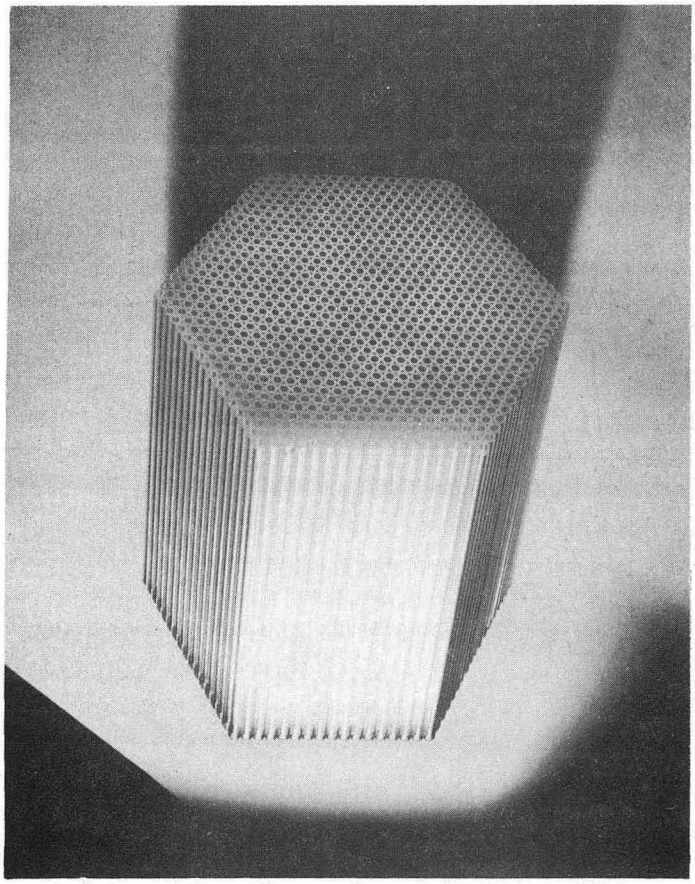

CBB 765-4207

Fig. 10

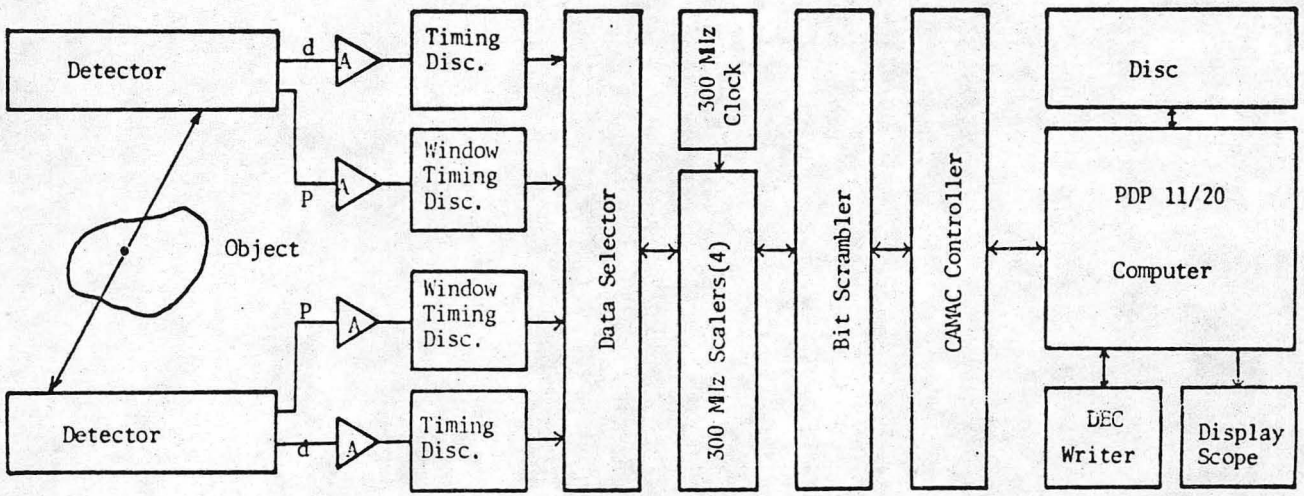

P = Prompt anode pulses

d = Delay line pulses

A = Amplifiers

Fig. 11

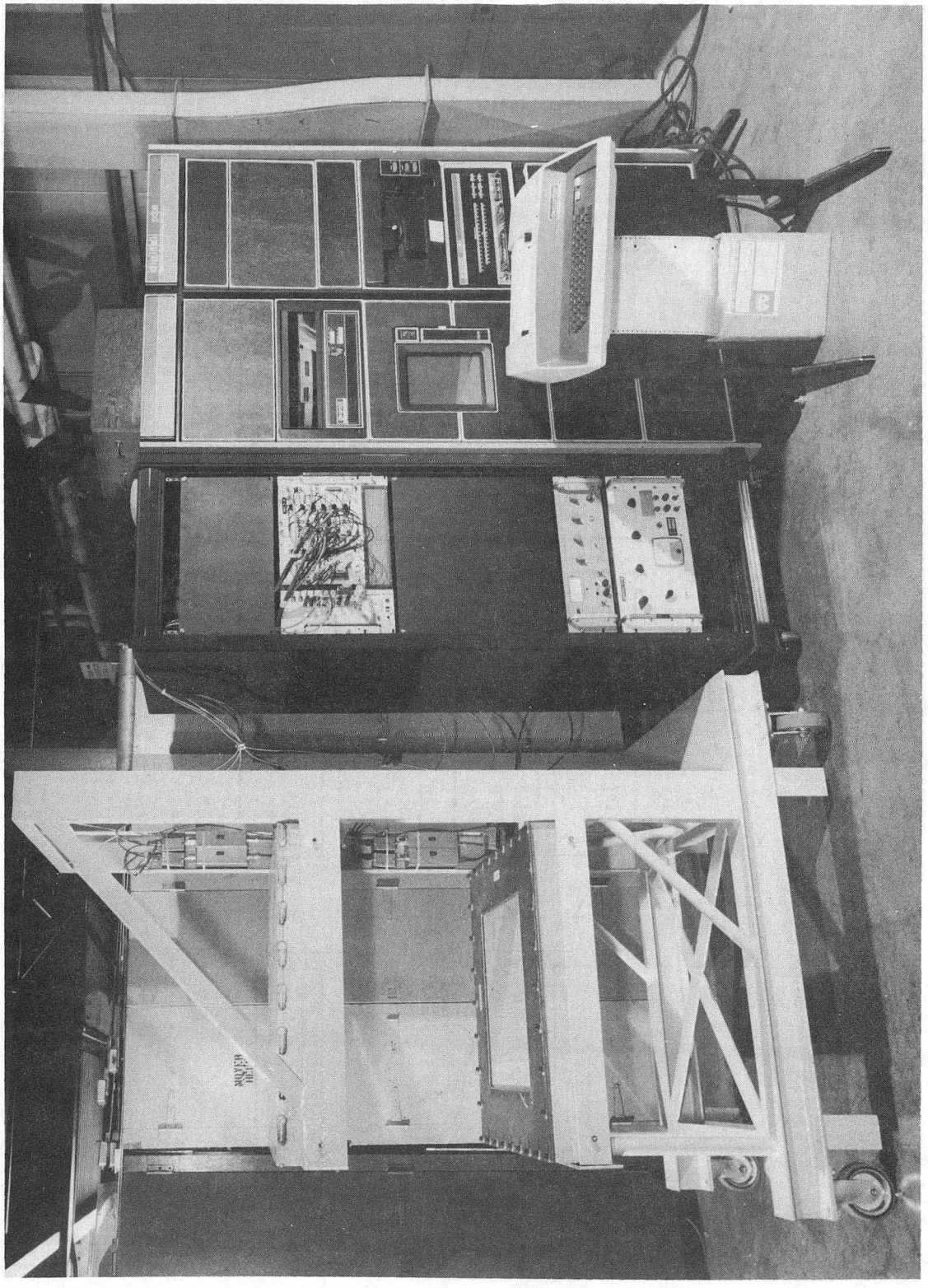

CBB 745-3643

Fig. 12

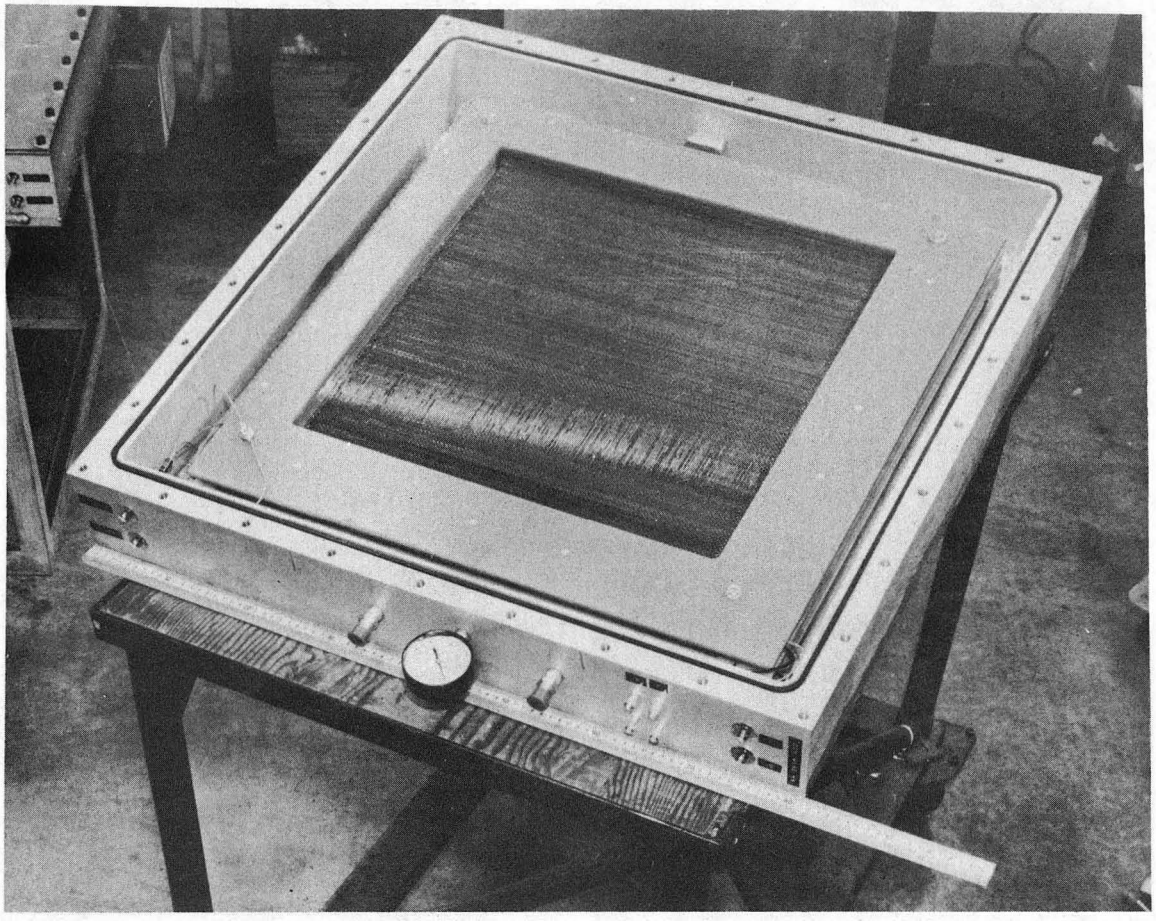

XBB 7410-7153

Fig. 13

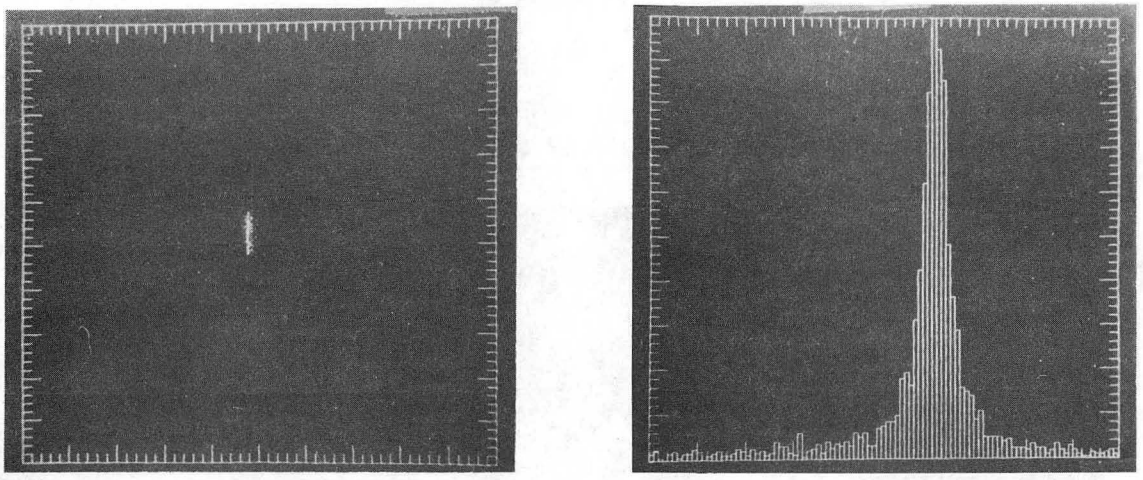

50 cm Full Scale
(a)

mm/bin
(b)

Fig. 14a.

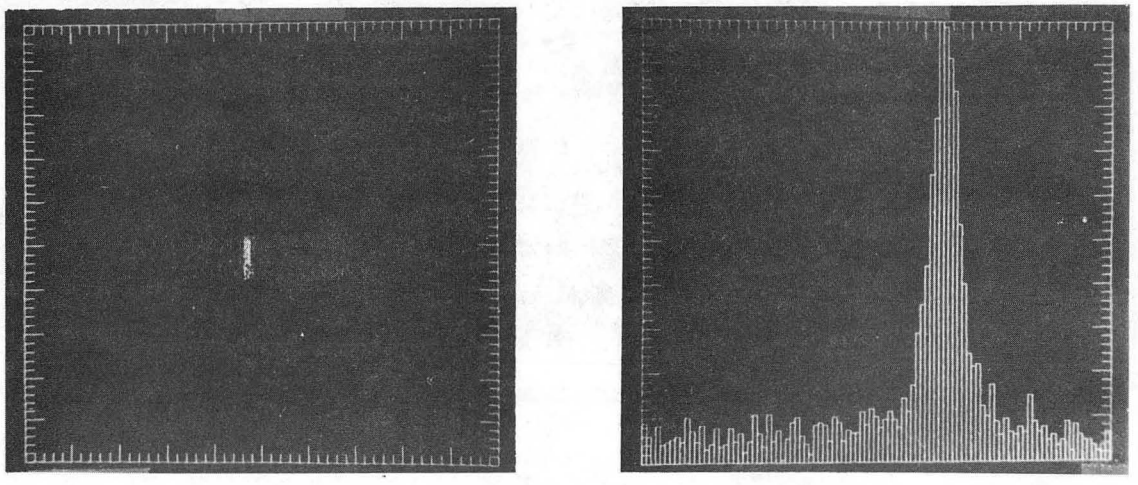

50 cm Full Scale
(a)

mm/bin
(b)

XBB 745-3590

Fig. 14 b.

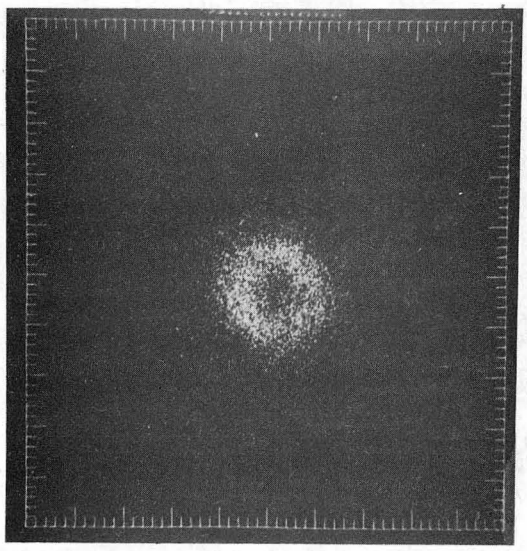

10 cm Full Scale

Fig. 15

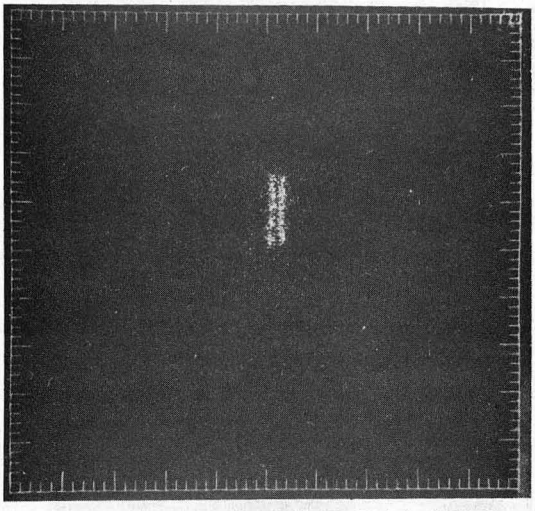

XBB 745-3591

50 cm Full Scale

Fig. 16

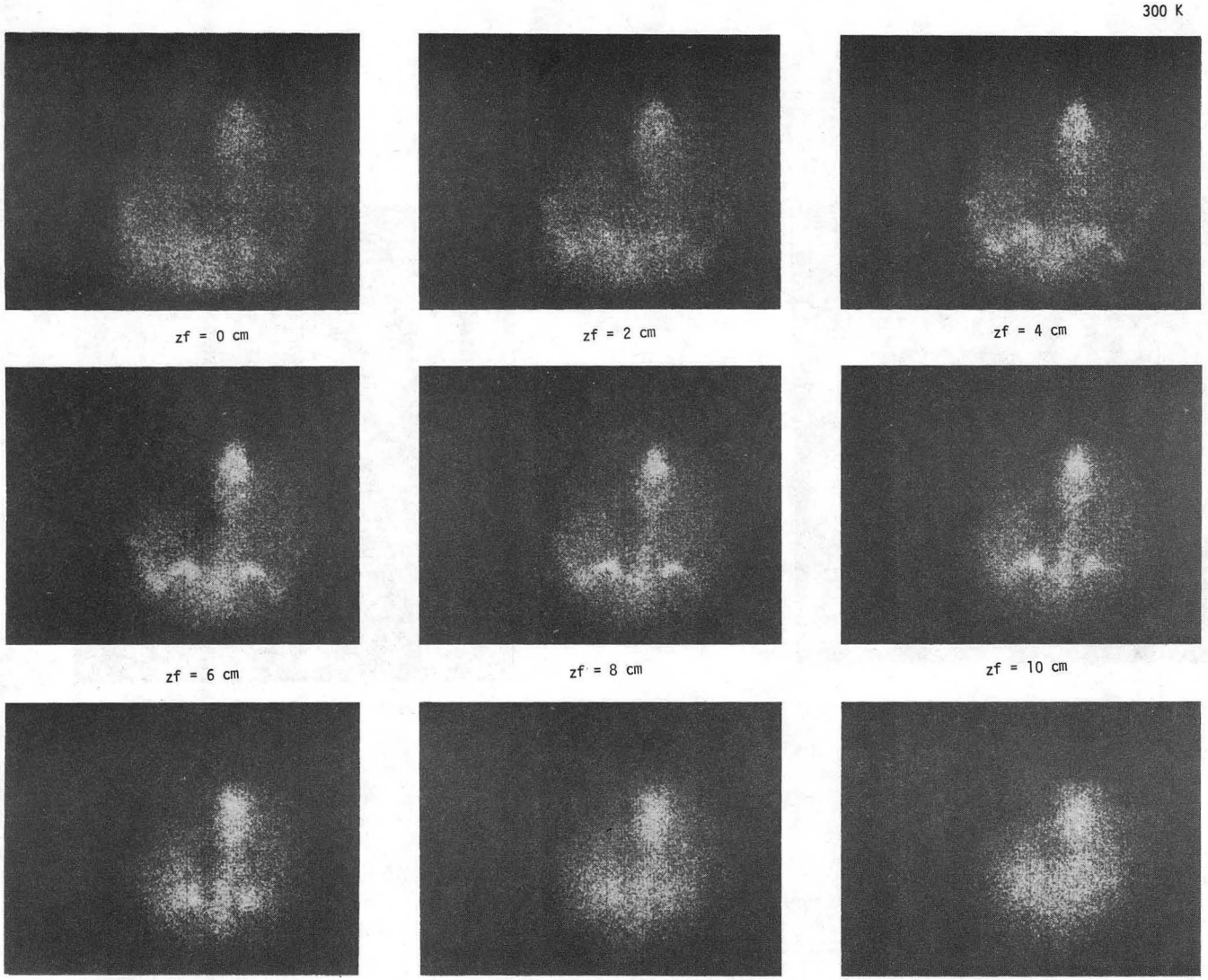

Fig. 17

XBB 748-5311

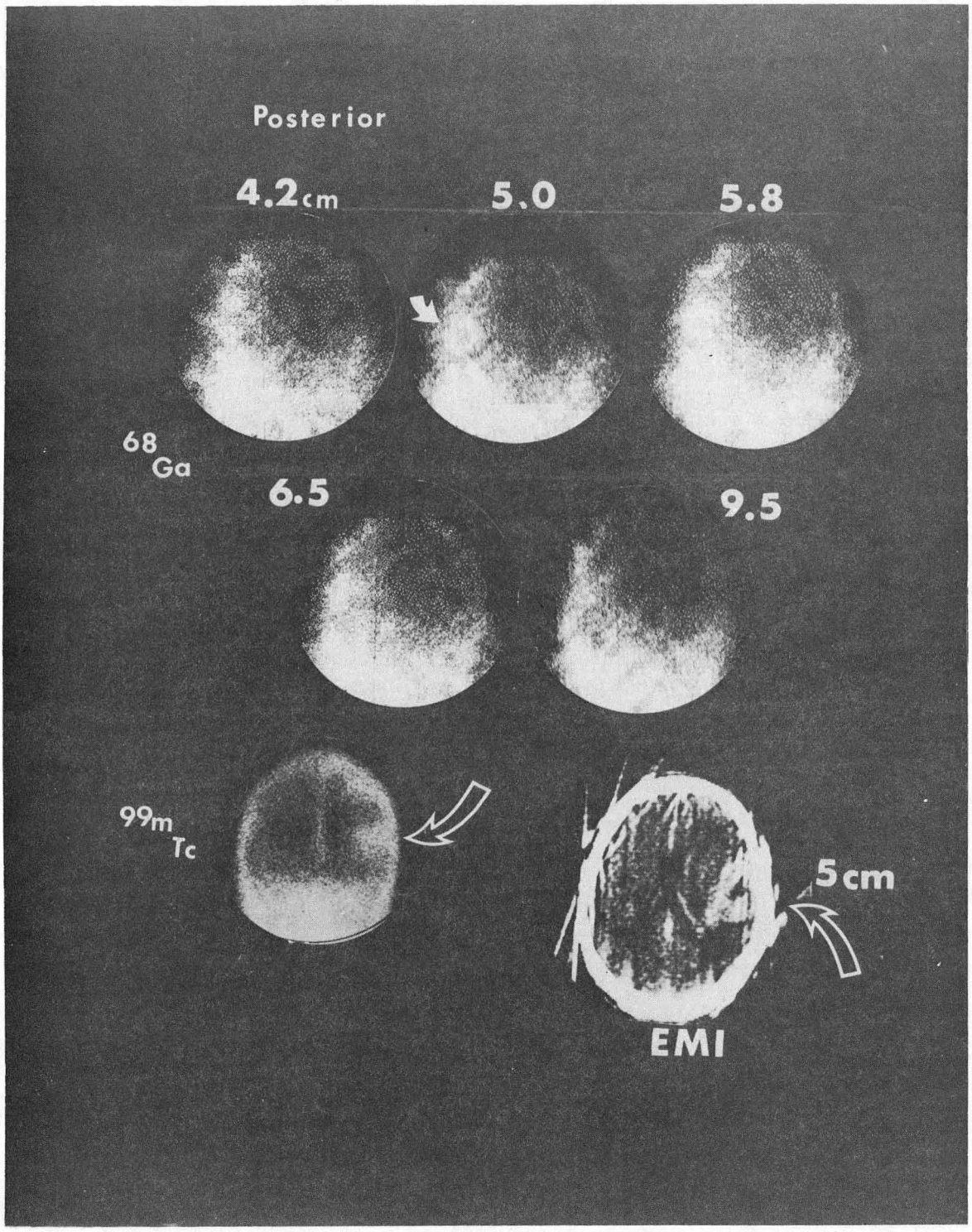

XBB 756-4145

Fig. 18

TECHNICAL INFORMATION DIVISION
LAWRENCE BERKELEY LABORATORY
UNIVERSITY OF CALIFORNIA
BERKELEY, CALIFORNIA 94720